# Crashworthiness simulation of multi-cell tubes under oblique impact loads

## \*Jianguang Fang, Guangyong Sun, †Qing Li

School of Aerospace, Mechanical and Mechatronic Engineering, The University of Sydney, Sydney, NSW 2006, Australia

> \*Presenting author: <a href="mailto:fangjg87@gmail.com">fangjg87@gmail.com</a> †Corresponding author: <a href="mailto:ging.li@sydney.edu.au">ging.li@sydney.edu.au</a>

#### **Abstract**

Multi-cell tubes have been drawn increasing attention for their excellent energy-absorbing ability. However, the effect of cell number and oblique loads on crashing behaviors is seldom studied to date. In this paper, a group of multi-cell tubes with different cell numbers are comprehensively investigated under both axial and oblique loads. The finite element models are first established and then validated by experimental tests. The simulation results show that the increase in cell number can be beneficial to the energy absorption (EA) but detrimental due to increase in peak force ( $F_{max}$ ) under axial load. When the oblique loads are taken into account, the tubes could undergo global bending, which is an inefficient deformation mode.

**Keywords:** Multi-cell tube; Oblique impact; Crashworthiness

## 1 Introduction

In automotive engineering, the bumper system requires to endure a load with a 30° loading angle to the longitudinal axis [1]. Under this condition, thin-walled structures always undergo a combined deformation of bending and axial crushing, rather than pure axial collapse that is designed as an efficient deformation mode for energy absorption. Due to the presence of global bending, the energy absorption of thin-walled structures can be reduced dramatically. For this reason, oblique loading has to be considered in crashworthiness design for thin-walled structures. For this purpose, Han and Park [2] investigated the crush behavior of a square column subjected to oblique loads and found that the loading angle has considerable effect on deformation pattern from the axial buckling to global bending. Reves et al. [1, 3, 4] studied the crashworthiness performance of hollow and foam-filled aluminum tubes under quasi-static oblique loads by using experimental and numerical methods. Zarei and Kröger [5] performed axial and oblique impact tests on empty and aluminum honeycomb filled square tubes and observed a dramatic decrease in first peak load during the oblique impact test. Tarlochan et al. [6] proposed a design process for a thin-walled structure subjected to both axial and oblique loads and found that the hexagonal profile was a better choice for energy absorption application. Yang and Qi [7] developed an optimization procedure for design of the empty and foam-filled square columns under oblique loading and the results showed that compared with the foam-filled tubes, the empty column can behave better under oblique impact but worse under pure axial loading. To be the author's best knowledge, there have been very limited studies of multi-cell tubes to take into account the oblique loads so far. Qi et al. [8] employed LS-DYNA to predict the crashing behaviors of four tubes with different cellular configurations under oblique loads, and they found that multi-cell tapered tube has the best crashworthiness performance. Song and Guo [9] found that the effectiveness of multi-cell configuration for improving tubes' energy absorption reduces as the load angle increases, and multi-cell tubes can even have worse performance if they collapse in global bending mode.

From the abovementioned studies, it is known that comprehensive comparison of the crashworthiness of multi-cell structures with different cell numbers remains under-studied thus far. Furthermore, how does the cell number affect the crashworthiness under oblique loads? This study aims to address these two issues.

# 2 Numerical modeling

# 2.1 Finite element (FE) model

The structures to be analyzed here comprise a group of thin-wall multi-cell square tubes with the same axial length of L=200 mm and the same width of b=75mm subjected to oblique impact loading (Fig. 1). These square tubes have different cell numbers (i.e., N×N=1×1, 2×2, 3×3, ..., 10×10), and are assigned different thicknesses in order to investigate these tubes with the same mass (Fig. 1). As shown in Fig. 2, a rigid wall with a mass of 600 kg and an incident angle  $\theta$  impacts on the top end of the tubes at an initial velocity of v= 15 m/s. the bottom ends of the tube is attached to the fixed rigid ground.

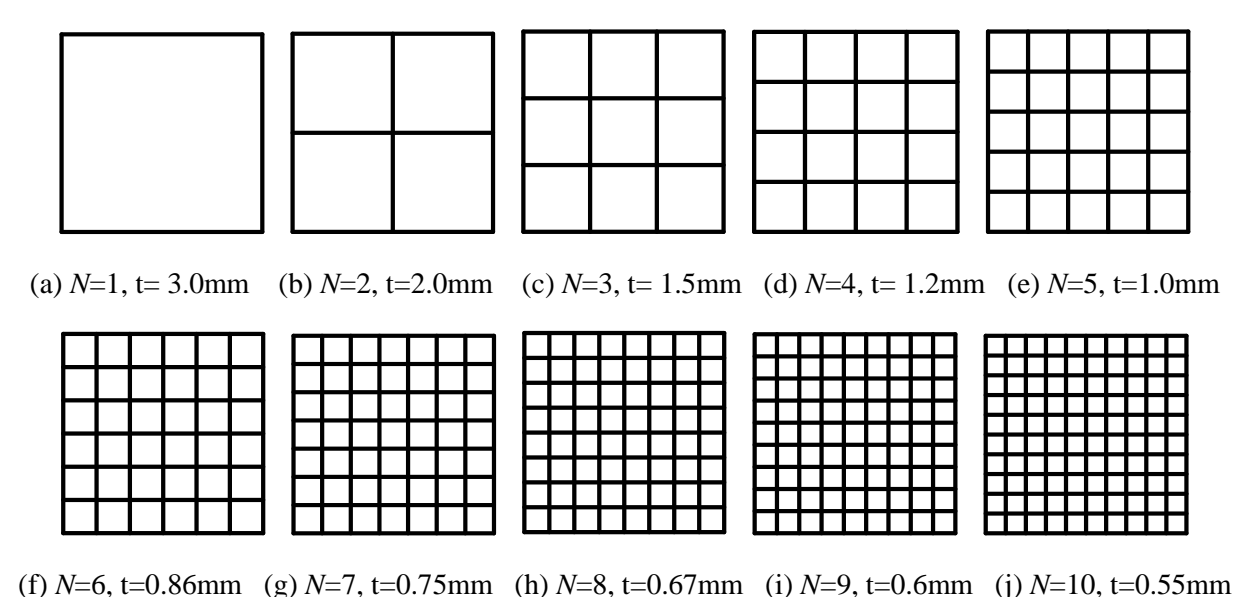


Fig. 1 Cross-sections of multi-cell tubes with the same mass but different wall thicknesses.

The numerical models are developed using explicit non-linear finite element code LS-DYNA. The Belytschko-Lin-Tsay reduced integration shell elements with five integration points through the thickness were employed to model the tubes. Stiffness-based hourglass control was employed to avoid spurious zero energy deformation modes and reduced integration was used to avoid volumetric locking. The interfaces between the tube and rigid wall and between the tube and rigid ground were both modeled as an "automatic node to surface". "Automatic single surface" contact was also prescribed to the tube to avoid interpenetration during tube folding. For both

static and dynamic friction, the friction coefficient of 0.2 was adopted for all contact conditions [10-12].

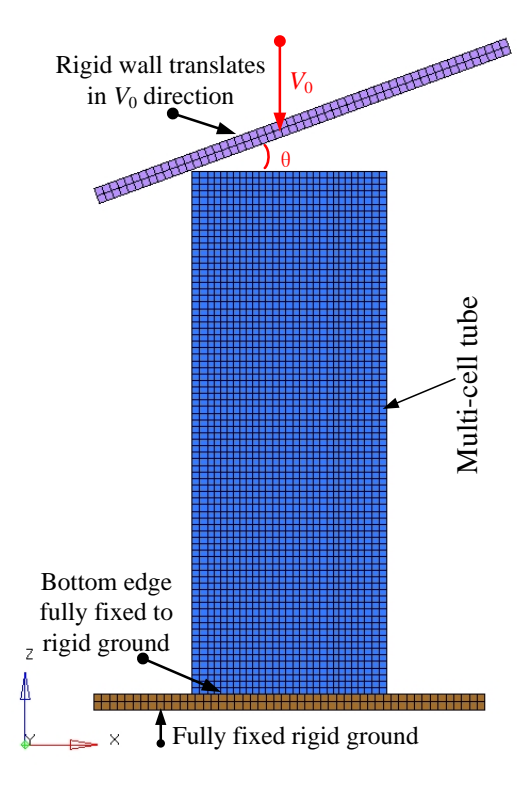


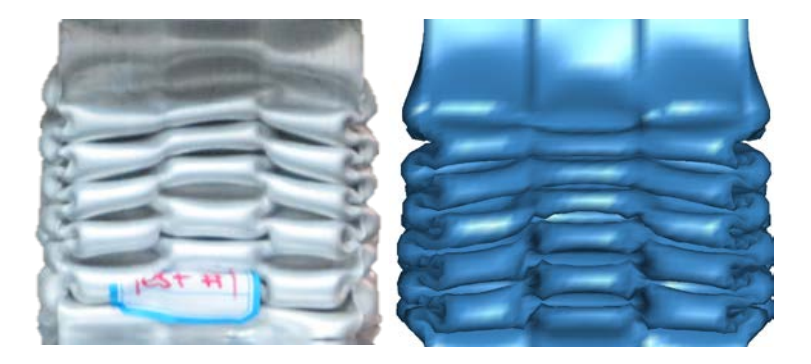
Fig. 2 Finite element model of multi-cell tube subjected to oblique loading.

The tube was modeled through a piecewise linear elastic-plastic behavior with strain hardening (material model 24 in LS-DYNA). The thin wall material was aluminum alloy AA6063-O with the density =2700 kg/m<sup>3</sup>, Poisson's ratio =0.3, and Young's modulus =70 GPa. The material model was considered insensitive to strain rate but defined as non-linear isotropic work hardening in the plastic region [13, 14].

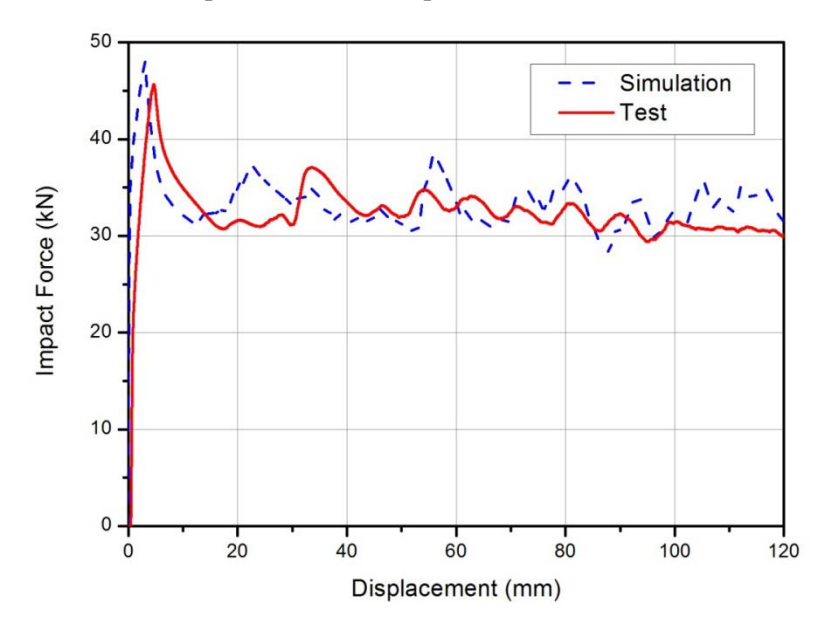
## 2.2 Validation of FE modeling

In order to validate the FE modeling, a tube with 3×3 uniform cells was compressed using the available test facilities with a constant axial impact velocity of 3mm/min. The simulation model with the same specimen configuration was established under the same testing conditions. Fig. 3(a) depicts a comparison of the deformed shapes between the FE simulation and experimental tests. The overall profile of FE model in terms of the collapse mode and number of folds is in good agreement with the experiment. Fig. 3(b) illustrates a comparison of the FE and experimental results of the load-displacement responses, in which a fairly good overall agreement between them is observed. From which, it is easily found that the maximum discrepancy of initial peak force is less than 5% and the FE prediction exhibits a slightly higher peak load than the experiment during the subsequent folding. This could be attributed to that the existence of imperfections in the physical specimen, which is difficult to be considered precisely in FE

modeling. Overall, the numerical modeling technique adopted here is considered sufficiently accurate and will be extended to the subsequent study.



(a) Comparison of deformation profile between experimental test (left) and numerical model (right)



(b) Force – deformation curves from experimental test and FE modeling

Fig. 3 Comparison of experimental and simulation results.

# 3 Crashworthiness of multi-cell tubes under different load angles

To systematically measure the crashworthiness of different structures, many different indicators have been proposed [15, 16], of which the energy absorption (*EA*) denotes the absorbed energy via plastic deformation of structures as

$$EA = \int_0^\delta F(\mathbf{x}) dx \tag{10}$$

where  $F(\mathbf{x})$  is the instantaneous crushing force in axial direction.  $\delta$  denotes the crash displacement, which is taken as 0.6L in this study, and L=200mm is the tube length.

In addition to energy absorption, crushing forces designate other key crushing criteria, of which peak crushing force ( $F_{\text{max}}$ ) represents the maximum value of  $F(\mathbf{x})$  and the mean crushing force (MCF) measures level of average crushing force given as

$$F_{avg} = \frac{EA}{\delta} = \frac{\int_0^{\delta} F(\mathbf{x}) dx}{\delta}$$
 (11)

Besides, crushing force efficiency (CFE) is also used as an indicator given as:

$$CFE = \frac{F_{avg}}{F_{max}} \times 100\% \tag{12}$$

Note that a large  $F_{\rm max}$  often leads to a high deceleration and high risk of severe injury or even death of occupant when impact occurs. Besides, the higher the *CFE* value, the better the load uniformity for an energy absorber. In this paper, these abovementioned indictors will be considered under oblique and axial loads.

## 3.2 Results of pure axial crushing

Fig. 4 displays the deformations of multi-cell tubes with the different cell numbers of  $1\times1$ ,  $4\times4$ ,  $7\times7$  and  $10\times10$  (i.e., N=1, 4, 7 and 10) under pure axial loads respectively, and Fig. 5a depicts the corresponding crushing force curves. For single cell structure (N=1), it can be seen that the crushing force first reaches an initial peak, followed by a dramatic drop and then fluctuates at some low values that correspond to the progressive folding. When cell number N increases, the crush force does not increase noticeably in the initial peak and tends to be stable during the whole crushing displacement. Specifically, the difference between the initial peak and the following peaks becomes small, and the force tends to fluctuate within a narrow range when cell number N increases. This might be attributed to that the fold length (the distance between two adjacent plastic hinges) decreases and thus the fold number increases with the increase in N (as shown in Fig. 4).

From Fig. 6(a) it can be seen that under the same mass the EA increases as the cell number increases, but the increased value become smaller and smaller, which represent that the energy absorption becomes stable gradually. From Fig. 6(b), the value of  $F_{\rm max}$  increases fairly slowly when the cell number increases, indicating that  $F_{\rm max}$  is insensitive to the cell number under the pure axial load condition. As for the CFE, its value increases when N<4 and then oscillates when N>4.

#### 3.3 Results of oblique crushing

From Fig. 4, the deformation modes of tubes the oblique impact of  $\theta$ =10° are fairly similar to those of  $\theta$ = 0°. That is to say that when the tubes are subjected to the oblique impact with a small incident angle, they are still able to generate proper progressive folding in the axial direction, which is typically regarded as an efficient deformation pattern. Interestingly, the impact forces fluctuate within a fairly small range after the initial peaks when  $\theta$  increases from 0 to 10° (Fig. 5(b)). Similarly to the situations of  $\theta$ = 0°, the more the cells of the tube has, the larger the force

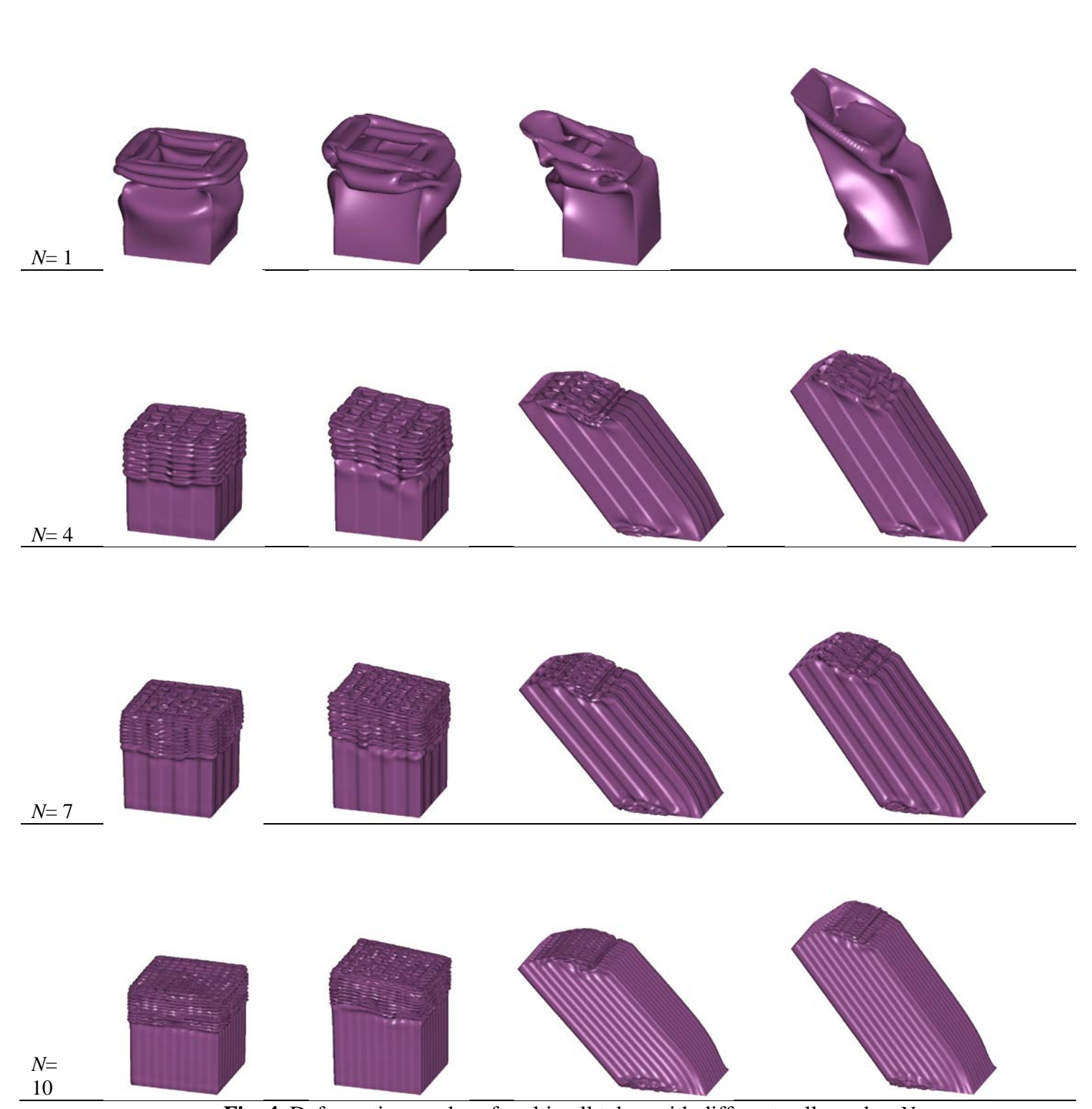
bears during the impact. As a result, it is observed from Figs. 8(a) and 8(b) that the increase in cell number N leads to the increase of  $F_{\text{max}}$  and EA. Besides, the  $F_{\text{max}}$  and EA of all tubes both decrease when  $\theta$  increases from 0° to 10°; and the  $F_{\text{max}}$  decreases more than EA does, which well explains why the CFE of  $\theta$ =10° is larger than that of  $\theta$ =0° for each tube (Fig. 6(c)), since the EA is equivalent to  $F_{\text{avg}}$  (see Eq.(11)).

When  $\theta$  increases to  $20^{\circ}$ , the global bending mode is observed for the tubes with more cells (N> 2). The compression flange buckles and develops a plastic hinge close to the clamped distal end (in N=4, 7, 10 in Fig. 4). Then the whole tube bends around this hinge as almost an rigid body motion. On the other hand, the tubes with a smaller cell number (e.g. N= 1 and 2) still succeed to avoid such a global bending. From Fig. 5(c), the tubes of N= 4, 7 and 10 reach a peak load and then decrease dramatically due to the global bending, weakening the energy absorption and load-carrying capacity. As a result, Figs. 8a and 8b exhibit that the EA and  $F_{max}$  of N= 4, 7 and 10 reduce much more when  $\theta$  increases from 10° to 20°, compared with those of N= 1 and 2. When  $\theta$  increases up to 30°, global buckling occurs in all the tubes (Fig. 4) and the EA and  $F_{max}$  become even smaller (as Figs. 8(a) and 8(b)). Interestingly, from Fig. 5(d), the tube of N= 1 undergoes a longer deformation before the impact force decreases significantly, representing that it bends later than the other three.

Overall, when multi-cell tubes are impacted obliquely with a small loading angle  $\theta$ , all of them collapse progressively in the axial direction, which is very similar to the situation in pure axial loading. When  $\theta$  increases, multi-cell tubes begin to bend globally, which leads to reduction of load-carrying and energy absorption. It can also be seen that the tubes with more cells are more sensitive to oblique loads, although they succeed to absorb more energy in pure axial case and oblique case with small angle  $\theta$ .

#### 4 Conclusions

In this study, the crashing behaviors of multi-cell tubes with ten different cell numbers have been comprehensively investigated under both axial and oblique loads. The simulation models were established using non-linear finite element code LS-DYNA and then validated by experimental test. It was found that both energy absorption (EA) and peak force ( $F_{max}$ ) of multi-cell tubes increase with the increase in cell number under axial loads. Regarding the oblique loads, the tubes can remain to collapse progressively in axial direction when the incident angle ( $\theta$ ) is small, but they develop global bending when  $\theta$  increases up to  $20^{\circ}$  and  $30^{\circ}$ . It was also observed that the tubes with fewer cells are more robust to oblique loads with large angle but perform worse under pure axial load than the tubes with more cells.



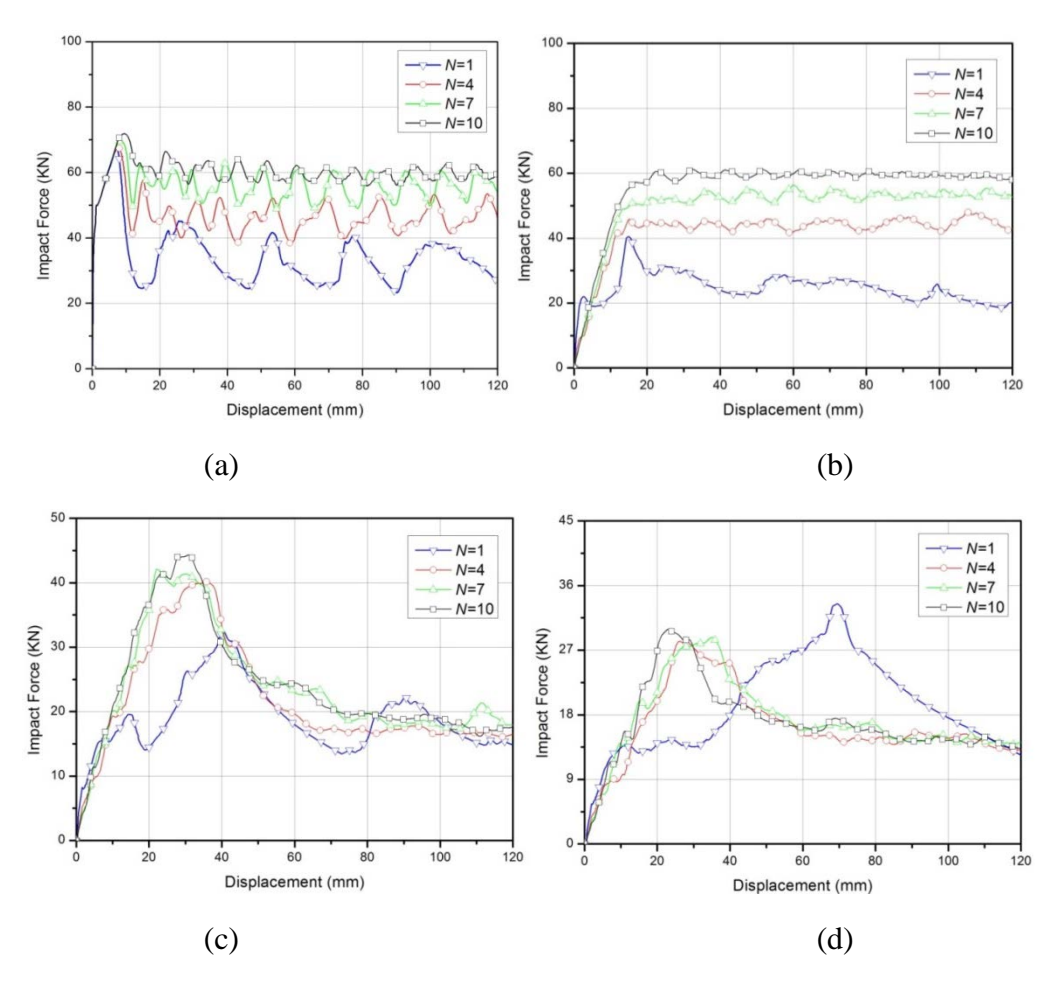
*θ*= 20°

*θ*= 30°

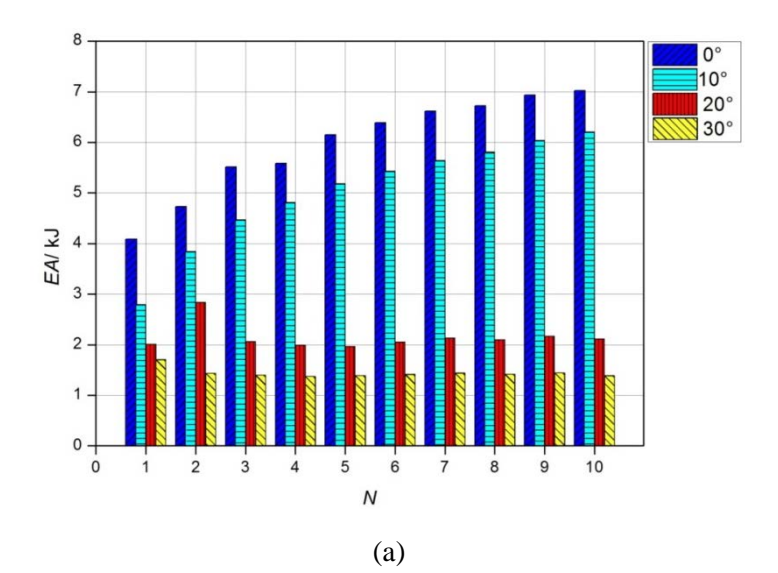
*θ*= 10°

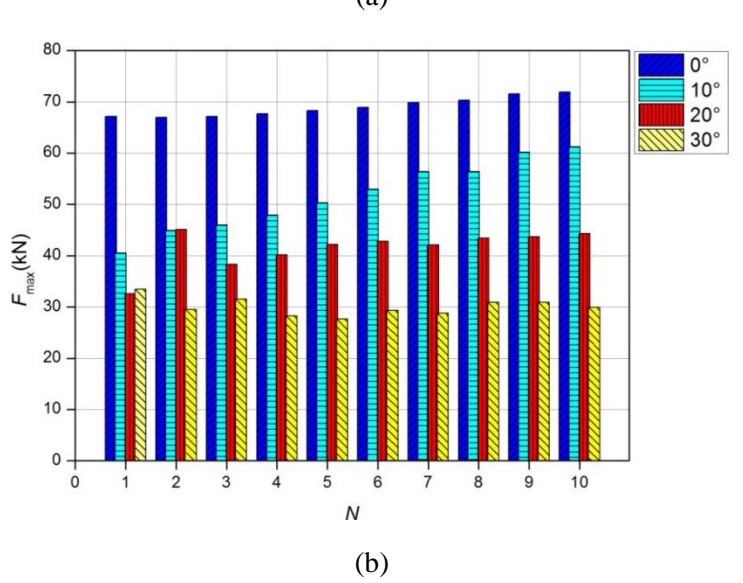
*θ*= 0°

Fig. 4 Deformation modes of multi-cell tubes with different cell number N



**Fig. 5** Crashing force vs. displacement curve: (a)  $\theta$ = 0°, (b)  $\theta$ = 10°, (c)  $\theta$ = 20°, (d)  $\theta$ = 30°.





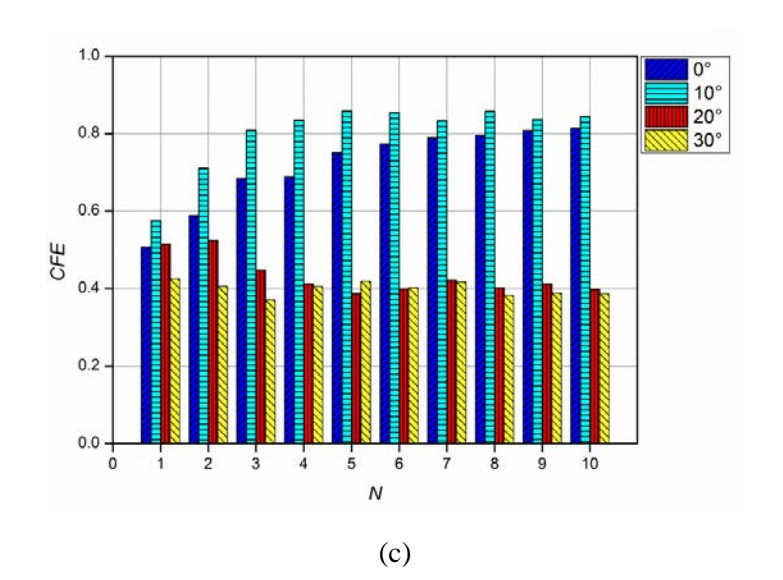


**Fig. 6** Performance comparisons under different loading angles: (a) EA, (b)  $F_{max}$ , (c) CFE.

#### References

- [1] A. Reyes, M. Langseth, O. Hopperstad, Crashworthiness of aluminum extrusions subjected to oblique loading: experiments and numerical analyses, Int J Mech Sci, 44 (2002) 1965-1984.
- [2] D. Han, S. Park, Collapse behavior of square thin-walled columns subjected to oblique loads, Thin Wall Struct, 35 (1999) 167-184.
- [3] A. Reyes, M. Langseth, O. Hopperstad, Square aluminum tubes subjected to oblique loading, Int J Impact Eng, 28 (2003) 1077-1106.
- [4] A. Reyes, O. Hopperstad, M. Langseth, Aluminum foam-filled extrusions subjected to oblique loading: experimental and numerical study, Int J Solids Struct, 41 (2004) 1645-1675.
- [5] H. Zarei, M. Kröger, Optimum honeycomb filled crash absorber design, Mater Design, 29 (2008) 193-204.
- [6] F. Tarlochan, F. Samer, A.M.S. Hamouda, S. Ramesh, K. Khalid, Design of thin wall structures for energy absorption applications: Enhancement of crashworthiness due to axial and oblique impact forces, Thin Wall Struct, 71 (2013) 7-17.
- [7] S. Yang, C. Qi, Multiobjective optimization for empty and foam-filled square columns under oblique impact loading, Int J Impact Eng, 54 (2013) 177-191.
- [8] C. Qi, S. Yang, F.L. Dong, Crushing analysis and multiobjective crashworthiness optimization of tapered square tubes under oblique impact loading, Thin Wall Struct, 59 (2012) 103-119.
- [9] J. Song, F.L. Guo, A comparative study on the windowed and multi-cell square tubes under axial and oblique loading, Thin Wall Struct, 66 (2013) 9-14.
- [10] H.F. Yin, G.L. Wen, Z.B. Liu, Q.X. Qing, Crashworthiness optimization design for foam-filled multicell thin-walled structures, Thin Wall Struct, 75 (2014) 8-17.
- [11] Z. Zhang, S. Liu, Z. Tang, Crashworthiness investigation of kagome honeycomb sandwich cylindrical column under axial crushing loads, Thin Wall Struct, 48 (2010) 9-18.
- [12] Z. Tang, S. Liu, Z. Zhang, Analysis of energy absorption characteristics of cylindrical multi-cell columns, Thin Wall Struct, 62 (2013) 75-84.
- [13] J. Fang, Y. Gao, G. Sun, Y. Zhang, Q. Li, Parametric analysis and multiobjective optimization for functionally graded foam-filled thin-wall tube under lateral impact, Computational Materials Science, 90 (2014) 265-275.
- [14] J. Fang, Y. Gao, G. Sun, Y. Zhang, Q. Li, Crashworthiness design of foam-filled bitubal structures with uncertainty, International Journal of Non-Linear Mechanics, 67 (2014) 120-132.
- [15] G. Sun, G. Li, S. Hou, S. Zhou, W. Li, Q. Li, Crashworthiness design for functionally graded foam-filled thin-walled structures, Materials Science and Engineering: A, 527 (2010) 1911-1919.
- [16] M.A. Guler, M.E. Cerit, B. Bayram, B. Gerceker, E. Karakaya, The effect of geometrical parameters on the energy absorption characteristics of thin-walled structures under axial impact loading, International Journal of Crashworthiness, 15 (2010) 377-390.